Influence of pH and Proton Donor/Acceptor Identity on Electrocatalysis in Aqueous Media

Vincent J. Ovalle and Matthias M. Waegele*

Department of Chemistry, Merkert Chemistry Center, Boston College, Chestnut Hill, Massachusetts 02467, United States

E-mail: waegele@bc.edu

Abstract

Understanding the effects of solution pH on the rates and mechanisms of multiproton/electron transfer reactions at aqueous electrolyte/electrode interfaces has been an active area of research for many decades. Recent interest in this topic has been driven by observations that the reaction selectivity and rates of electrocatalytic processes for energy storage and renewable fuel synthesis can profoundly change with electrolyte pH. Further, a subset of these reactions, such as CO and CO₂ reduction, are often carried out under near-neutral bulk pH conditions. Such conditions, in combination with insufficient mass transport and limited pH buffer capacity, can lead to substantial deviations of the near-electrode pH from the bulk pH of the electrolyte. Such pH gradients, together with electrodes whose surface chemistry is highly dependent on pH, can give rise to complex feedback between the reactions that are catalyzed on the surface and the local pH conditions and surface speciation. In this Perspective, we discuss representative studies that characterize and quantify the effects of (local) pH on electrocatalysis with innovative experimental and theoretical methods. further highlight possible future directions of investigation.

Introduction

Electrocatalytic reactions involving the transfer of multiple protons and electrons at an aqueous electrolyte/electrode interface play a central role in electrochemical energy conversion. The hydrogen evolution reaction (HER), ^{1,2} oxygen reduction reaction (ORR), 3,4 CO/CO₂ reduction reactions, 5,6 ammonia oxidation reaction, ^{7,8} formic acid oxidation, ^{9,10} and oxygen evolution reaction (OER)^{11,12} are examples of such processes. At a fixed reversible hydrogen electrode (RHE) potential (U_{RHE}) , that is, at a fixed overpotential, the rates and selectivity of such reactions often exhibit complex dependence on electrolyte pH. 13 Therefore, it is of particular importance to understand the mechanisms by which the pH can alter the energetics of competing electrocatalytic pathways. Generating this understanding is a complex task as the pH can influence electrocatalysis in a multitude of ways: For example, at a fixed $U_{\rm RHE}$, a change in pH alters the charge density on an electrode, which can modulate the adsorption energies of reaction intermediates; ^{14,15} the pH also often determines the surface speciation by influencing the site preference of reaction intermediates or by controlling the stability of surface phases; 16,17 the identity and concentration of proton donor and acceptor can have a significant impact on the reactions and can change with pH. 18,19 Apart from this diversity of pathways in which the electrolyte pH can affect electrocatalytic processes, the iden-

tification of these mechanisms is further complicated by the interdependence of the pH in the vicinity of the electrode (local pH) and the electrocatalytic process. In particular, multielectron/proton transfer reactions catalyzed at near-neutral bulk pH can bring about changes in local pH by several pH units due to fast production or consumption of protons in the electrocatalytic process. ^{20–25} Elucidating pH effects therefore requires experimental approaches that can probe local pH and pH-dependent surface speciation as well as theoretical techniques that can capture the pH-dependent properties of the interface. In the last few years, significant experimental and theoretical advances have been made in this regard. In this Perspective, we highlight several representative studies with a focus on those that have appeared in the last 2-3 years. Earlier studies are discussed in Koper's seminal article on the theory of multiple proton/electron transfer reactions. 13 Apart from a few exceptions, we primarily concentrate on metal-electrode catalysts. A comprehensive review of studies involving transition metal oxides or molecular catalysts is beyond the scope of this Perspective. For related pioneering studies on the pH-dependence of electron/proton transfer reactions promoted by molecular catalysts ^{26–28} and metal oxides, ^{29–32} the reader is referred to the respective articles.

Potential-Dependent Adsorption Energy and Decoupled $\mathrm{H^+/e^-}$ Transfer

The free energy change for an electrochemical reaction of the form

$$^*A + H^+ + e^- \rightleftharpoons ^*AH$$
 (1)

can be expressed as 13,33

$$\Delta G = G_{*AH} - G_{*A} - \frac{1}{2}G_{H_2} + 2.3k_BT \text{ pH} + eU_{SHE},$$
(2)

where G_{*AH} , G_{*A} , and G_{H_2} are the free energies of the surface-adsorbed intermediates *A and *AH, and that of hydrogen gas, respec-

tively. $U_{\rm SHE},\,e,\,k_{\rm B},\,{\rm and}\,\,T$ are the electrode potential versus the standard hydrogen electrode (SHE), positive elementary charge, Boltzmann constant, and absolute temperature, respectively. Most reactions of current interest, such as the $4e^-$ ORR to water, involve a sequence of steps of a form similar to reaction 1 and therefore feature two or more surface-adsorbed intermediates. If the G_{*X} terms do not significantly change with $U_{\rm SHE}$, the reaction free energy of each elementary step shifts by exactly the same amount $(eU_{RHE} = 2.3k_BT pH + eU_{SHE})$ with $U_{\rm SHE}$ and pH. As a result, the thermodynamic overpotential, defined as the $U_{\rm RHE}$ at which all steps become thermodynamically downhill, is independent of pH. That is, the reaction does not exhibit a pH-dependence on the RHE scale. However, there are numerous examples in which multi-proton/electron transfer reactions show a dependence on the pH on the RHE scale. 13 As described in this section, decoupled H⁺/e⁻ transfers and/or a dependence of the G_{*X} terms on $U_{\rm SHE}$ are possible mechanisms by which a reaction can acquire such a dependence.

As discussed by Koper,¹³ if a reaction involves a sequence of steps in which H^+ and e^- are transferred in a sequential rather than in a concerted manner, the thermodynamic overpotential will depend on pH. This dependence arises because the step involving only H^+ transfer does not depend on $U_{\rm SHE}$, whereas the e^- transfer step does not depend on pH. That is, the free energies of the decoupled steps have a different dependence on pH and $U_{\rm SHE}$. This behavior contrasts with the case in which all steps are concerted H^+/e^- transfers, as noted in the preceding paragraph.

A pathway involving only concerted $\mathrm{H}^+/\mathrm{e}^-$ transfer steps may still exhibit a pH-dependence on the RHE scale if, for example, the $G_{^*\mathrm{X}}$ terms are dependent on U_{SHE} . ^{14,15} Using density functional theory (DFT) methods, Henkelman and co-workers explored the dependence of the binding energies of intermediates of the ORR on U_{SHE} . ¹⁴ Figure 1A shows the dependence of the total system energy (electrode + adsorbate) as a function of U_{SHE} . The parabolic dependence of the total energy with U_{SHE} arises from the charge on the

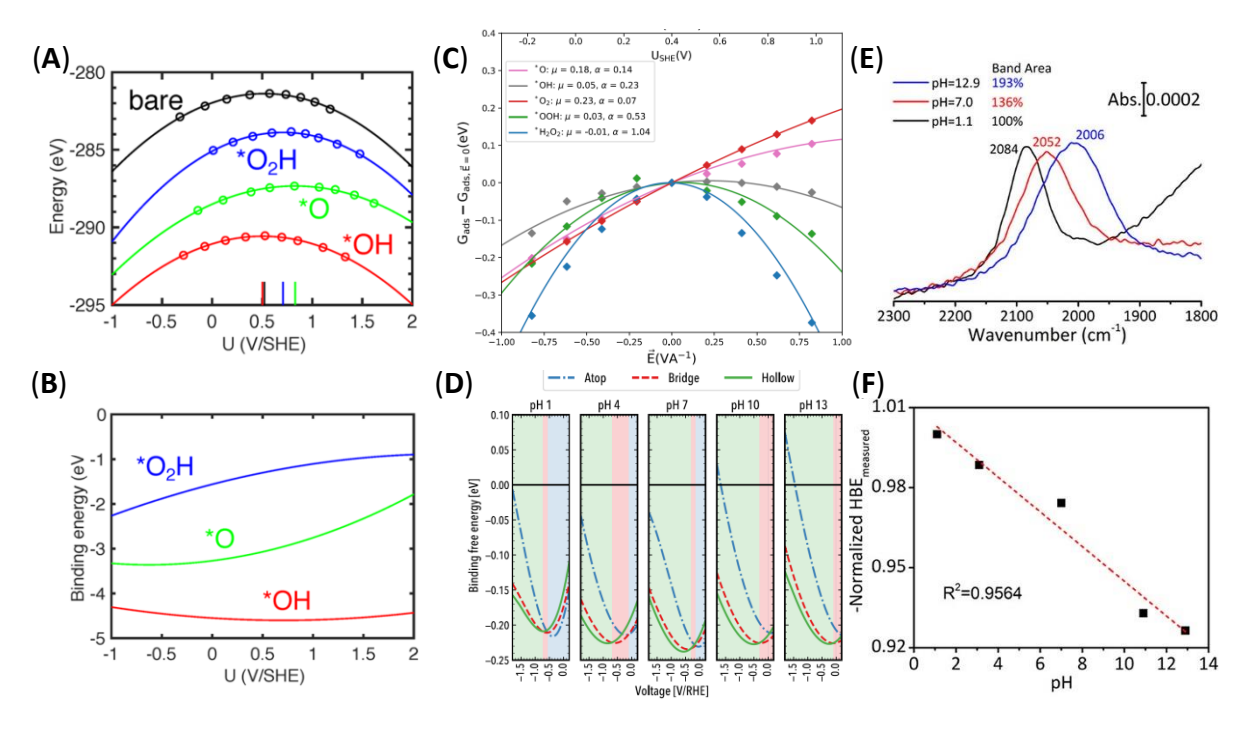


Figure 1: (A) Dependence of the total energies of bare Au(100) and Au(100) with *O_2H , *O_3 , and *O_3H on U_{SHE} . The maxima of the parabolas correspond to $U_{SHE,PZC}$, whose values are indicated as vertical lines for the different systems. Reprinted from reference 14. Copyright 2019 American Chemical Society. (B) Binding energies of adsorbates calculated as the difference in total energies between the bare and adsorbate-covered surfaces. Reprinted from reference 14. Copyright 2019 American Chemical Society. (C) Variation of adsorption energies of ORR intermediates on Au(100) with interfacial electric field strength, which is a function of U_{SHE} . Reprinted from reference 15. Copyright 2020 American Chemical Society. (D) CO binding free energies and site preference on Cu(100) as a function of U_{RHE} and pH. Reprinted from reference 17. Copyright 2020 American Chemical Society. (E) Pt-H stretch band at different electrolyte pH values as indicated. Reprinted from reference 34. Copyright 2020 American Chemical Society. (F) Relative hydrogen binding energy (HBE) derived from the peak frequency of the Pt-H stretch band as a function of pH. Reprinted from reference 34. Copyright 2020 American Chemical Society.

electric double layer capacitance whose energy is $\sim \frac{1}{2}C_{\rm dl}(U_{\rm SHE}-U_{\rm SHE,PZC})^2$, where $C_{\rm dl}$ is the double layer capacitance and $U_{\text{SHE,PZC}}$ is the potential of zero (free) charge of the electrode. As shown in Figure 1A, the $U_{\text{SHE,PZC}}$ values of the electrodes with the adsorbed species *O₂H and *O are more positive than that of the bare surface. Henkelman and co-workers attributed these shifts to the electron-withdrawing character of the two adsorbates, which shift the work function of the metal to more positive values. The difference between the total energies of the bare and adsorbate-covered surfaces give the potential-dependence of the adsorbate binding energy (Figure 1B). As a result of the significant shifts in $U_{\rm SHE,PZC}$ in the presence of *O₂H and *O, the binding energies of these adsorbates exhibit a dependence on $U_{\rm SHE}$. For a fixed $U_{\rm RHE}$, $U_{\rm SHE}$ shifts by $-2.3k_{\rm B}T$ pH with increasing pH. As a result of the more negative $U_{\rm SHE}$, the binding energy of *O₂H becomes more negative with increasing pH. It is important to note that this stabilization primarily occurs if the presence of the adsorbate significantly changes $U_{\rm SHE,\,PZC}$ and/or $C_{\rm dl}$. example, the binding energy of *OH is comparatively insensitive to $U_{\rm SHE}$ because *OH does not significantly change $U_{\text{SHE,PZC}}$ relative to that of the bare substrate (Figure 1A, B). Interestingly, they found that pre-adsorbed *OH amplifies the shifts in $U_{\text{SHE,PZC}}$ induced by *O₂H and *O. On the basis of these results, Henkelman and co-workers identified the stabilization of *O₂H in alkaline media as the cause of the promotion of the ORR in base.

In a related approach Chan, Nørskov, and co-workers considered the interaction of the ORR intermediates with the interfacial electric field. ¹⁵ In their model, the free energy of an intermediate is given by

$$G_{*X} = G_{*X}^{PZC} - \vec{\mu} \cdot \vec{E} - \frac{\alpha}{2} \vec{E}^2,$$
 (3)

where G_{*X}^{PZC} , $\vec{\mu}$, and α are the adsorbate's free energy at $U_{SHE,PZC}$, dipole moment, and polarizability, respectively. \vec{E} is the interfacial electric field. In this model, $U_{SHE,PZC}$ and C_{dl} are assumed to be independent of pH and the

presence of surface adsorbates. Accordingly, at a fixed U_{RHE} , pH effects in the ORR are due to the modulation of G_{*X} by the interaction of the adsorbates with the interfacial electric field (Figure 1C), $\vec{E} \sim C_{\rm dl}(U_{\rm SHE} - U_{\rm SHE, PZC})$, which becomes stronger as $U_{\rm SHE}$ shifts away from $U_{\rm SHE, PZC}$ with increasing pH. Their microkinetic model that includes the field-dependent free energies reproduces the trends seen in experimental polarization curves. The electric field effects predicted by equation 3 are expected to be particularly pronounced for reaction mechanisms that involve adsorbates with large dipole moments and/or polarizabilities, such as *CO₂ and *OCCO in CO₂ reduc $tion.^{35-37}$

In the examples discussed in the preceding two paragraphs, the binding site of the adsorbate does not change with potential or pH. However, changes in pH can also induce a change in site preference of a reaction intermediate, thereby modulating catalytic activity. Using a DFT-continuum approach, Weitzner, Varely, and co-workers probed the binding of CO as a function of pH and voltage on Cu electrodes. 17 Although typically considered a chemical step, changes in surface properties with applied potential render the adsorption of CO sensitive to the applied voltage. Their key findings include the following: (1) The site preference changes from atop > bridge > hollow sites at 0 V to hollow > bridge > atop at -1.5V versus RHE (Figure 1D). (2) The RHE potential at which this switch in site preference occurs shifts more positively with increasing pH (Figure 1D). (3) The degree to which the pH affects the adsorption energy of atop-bound CO depends on the nature of the site (kink, step edge, or terrace). Weitzner, Varely, and co-workers observed that K⁺ ions of the supporting electrolyte accumulate at the interface with decreasing potential, thereby increasing the absolute magnitude of the interfacial electric field. Accordingly, they suggested restructuring of the electrochemical double layer with voltage and pH as the origin of the observed site preference changes.

In earlier work, Janik and co-workers showed that at high pH, alkali metal cations can effectively compete with protons for adsorption sites on transition metal electrodes.³⁸ Because cations are known to affect electrocatalysis,³⁹ an apparent pH dependence of an electrochemical process can be rooted in cation effects.^{40–42}

pH-dependent adsorption energies have also been probed experimentally. For example, using surface-enhanced infrared absorption spectroscopy (SEIRAS), Shao and co-workers monitored the Pt-H stretch band as a function of pH at fixed $U_{\rm RHE}$. ³⁴ They found that the peak frequency of the Pt-H stretch band decreases with increasing pH (Figure 1E). Their analysis reveals that the *measured* binding energy linearly decreases by about 7.4% as the pH is increased from 1.1 to 12.9 (Figure 1F). They attributed this decrease in the measured binding energy to a combination of factors, including changes in electric field, *H coverage, Ptwater, and *H-water interactions. Shao and coworkers argued that the weakening of the Pt-H bond with increasing pH is one key factor that contributes to the lower HER rate under alkaline conditions. Related experimental and theoretical studies emphasized the pH-dependence of (1) the desorption energy of water, ^{43,44} (2) the structure of interfacial water, 45 and (3) the destabilization of surface-adsorbed hydroxide by cations 40-42 as possible origins for the observed modulation of the apparent hydrogen adsorption energies/potentials.

Finally, we note that Koper and co-workers attributed the slower kinetics of the HER in alkaline solutions to an increase in the reorganization energy for interfacial water with increasing pH. ⁴⁶ This increase in the reorganization energy arises from the stronger interfacial electric field with increasing pH. Using a nonfaradaic probe reaction during the HER, Surendranath and coworkers showed that the electrostatic potential at the Pt surface indeed increases by 60 mV per pH unit increase in the bulk pH. ⁴⁷ Interfacial electric fields can also be conveniently probed with vibrational Stark spectroscopy. ^{48–50}

Surface Speciation

In the preceding section, we discussed an example in which the preference of a reaction intermediate for a given type of catalytic site within the ensemble of available surface sites may change with pH. In the examples discussed so far, the surface phase of the electrode was assumed to be independent of pH. However, because of the pH-dependent stability of certain surface phases (such as oxides), structurally and chemically distinct active sites may be present on the surface in different pH regimes. 51-53 The opposite effect is also possible: The chemistry of some surface phases may influence the pH in the vicinity of the electrode. ⁵⁴ In the following, we will give a few representative examples in which the pH affects surface speciation (and vice versa).

Potential- and pH-induced surface reconstructions can contribute to changes in site preference. With SEIRAS, we observed a shift in the preferential binding site of adsorbed CO on polycrystalline Cu electrodes from an atop to a bridging configuration with increasing pH (Figure 2A, top). ⁵¹ We found that, in contrast to atop-bound CO (CO_{atop}), bridge-bonded CO (CO_{bridge}) is irreversibly adsorbed (Figure 2A, bottom) and inert to electrochemical reduction at an applied potential of -1.75 V versus SHE. Inspired by prior work that demonstrated that polycrystalline Cu electrodes form (111) and (100) facets under alkaline conditions and cathodic polarization, ⁵⁵ we attributed the change in binding preference to a pH- and potential-induced reconstruction of the elemental Cu electrode surface.

Subsequent studies highlighted the role of kinetically stable oxide phases in the observed changes in site preference. ^{52,53} Using in situ soft X-ray absorption spectroscopy to probe the Cu oxidation state and SEIRAS to determine the CO binding mode, Wu and co-workers demonstrated that only CO_{bridge} is observed on a Cu(0) dominant surface. ⁵² By contrast, CO_{atop} is the primary CO species on a Cu(I) dominant surface. CO_{atop} and CO_{bridge} co-exist on a surface that is composed of a mixture of Cu(I) and Cu(0). In a related study, Xu

and co-workers employed surface enhanced Raman spectroscopy (SERS) to understand the pH- and potential-dependent binding of CO on Cu. ⁵³ At a pH of 8.9, they observed only CO_{atop} during a linear potential sweep from 0.4 to -0.8V versus RHE. By contrast, at a pH of 10.6, a Raman band attributable to CO_{bridge} appears at $U_{\rm RHE}$ < -0.4 V, which closely coincides with the onset potential of Raman bands due to $CuO_x/(OH)_y$. At a pH of 12.6, the common onset potential of CuO_x/(OH)_y and CO_{bridge} shifts to -0.1 V and CO_{atop} is no longer observable at any potential. On the basis of these observations. Xu and co-workers concluded that an oxygen-containing surface phase promotes the binding of CO in a bridging configuration. Although the two studies differ in their detailed conclusions, they both demonstrate that pHdependent surface phases of metal electrodes can play an important role in determining the site preference of intermediate species. Such changes in surface composition can substantially alter the catalytic reactivity of the surface.

pH-dependent oxide phases may alter catalytic pathways. For example, the chemical identity of the prevalent oxide phase on Au oxide electrodes determines the reaction mechanism of the OER: Using SERS and CV analysis, Hetterscheid and co-worker determined the pHdependent oxide formation on an Au electrode surface with an " α -oxide" under acidic conditions and a " β -oxide" under basic conditions. ¹⁶ The α -oxide is attributable to an oxyhydroxide species that is stably formed under acidic conditions, while the β -oxide is Au(OH)₃ that preferentially forms in basic electrolyte. They found that in the pH range below 4, where the α -oxide dominates the surface, the onset potential of the OER on the RHE scale is independent of the pH (Figure 2B). This observation suggests a concerted proton and electron transfer in the rate-determining step. By contrast, at a pH higher than 10, the β -oxide becomes the predominant oxide phase. In this pH regime, the onset potential of the OER is pH dependent on the RHE scale. This pH-dependent onset potential is consistent with a mechanism in which proton and electron transfers are decoupled, as discussed in the previous section. In the intermediate pH regime between 4-10 both oxides coexist, and the two mechanistic pathways are simultaneously operational.

The above examples demonstrate how the electrolyte pH can influence surface speciation. The opposite case has also been observed: Surface species can alter the local pH. Using SERS, Kenis, Gewirth, and co-workers determined the local pH within ~ 3 nm of the surface of an electro-deposited Cu gas diffusion electrode (GDE) in an alkaline flow electrolyzer for CO₂ reduction.⁵⁴ Based on the pH-dependent equilibrium of carbonate and bicarbonate, they used the ratio of the respective Raman signals to assess the local pH. In 1 M KOH, they observed that the local pH decreases approximately linearly with decreasing potential, approaching a value about ~ 5 units lower than the bulk pH (Figure 2C). The monotonic decrease in pH even occurs in a potential range where no appreciable reduction of CO₂ takes place. The Raman spectra further reveal the presence of Cu₂CO₃(OH)₂ (malachite) under the experimental conditions. Accordingly, Kenis, Gewirth, and co-workers attributed the lower local pH to the reaction of carbonate and hydroxide with soluble Cu(II) to form insoluble malachite. They further showed that the soluble Cu(II) species originate from the dissolution of surface Cu oxide phases under these conditions. After reduction of the malachite and/or oxide layers, the interfacial pH increases to >11.

Roldan Cuenya and co-workers demonstrated a method in which the local pH, and as a result the selectivity of CO₂ reduction, is modulated by the periodic formation of a surface oxide species. ⁵⁶ They alternated $U_{\rm RHE}$ of a GDE in contact with 1 M KOH between -0.7 V and an anodic voltage, $E_{\rm an}$, in the range 0.6 to 1.5 V once every second and monitored the CO₂ reduction products formed. For pulse sequences with $E_{\rm an}=0.9$ V, they observed a moderate enhancement of C₂ product formation compared to the product spectrum for electrolysis at a constant $U_{\rm RHE}$ of -0.7 V without excursions to anodic potentials (Figure 2D). On the basis of extensive microscopic, spectroscopic, and electrocatalytic characterization, they attributed

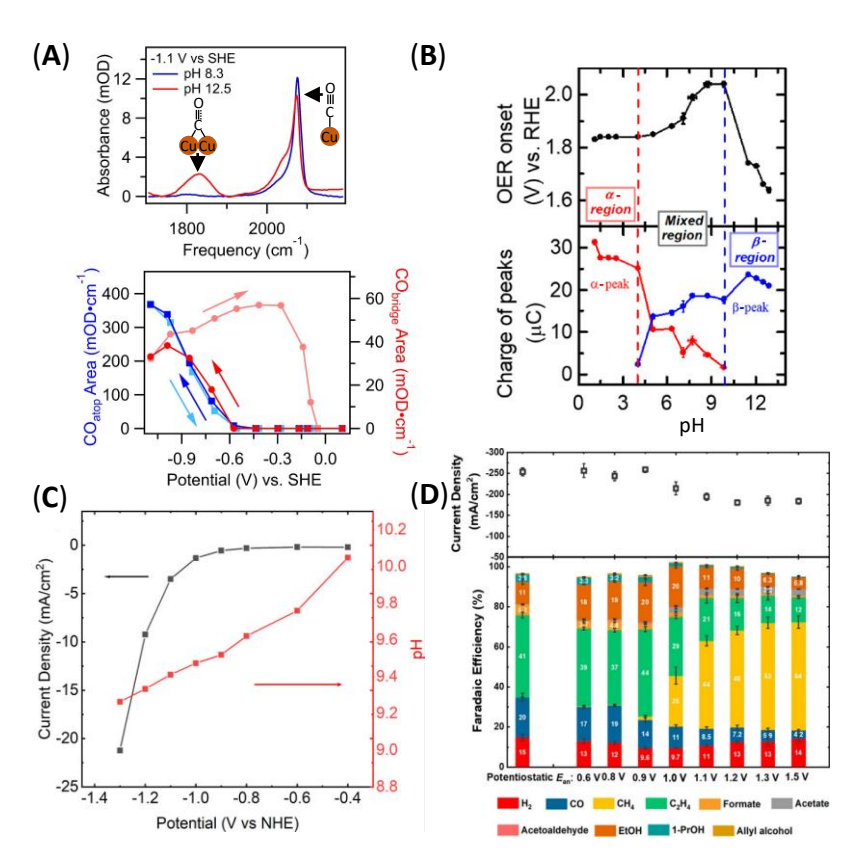


Figure 2: (A) pH-dependent spectra of adsorbed CO on Cu at -1.1 V versus SHE (top) and potential-dependent integrated band areas of the two observed adsorbed CO populations (bottom). Bottom panel Reprinted from reference 51. Copyright 2018 American Chemical Society. (B) Onset potential of the oxygen evolution reaction (top) and integrated charges of the α - and β -oxide reduction peaks as a function of pH. Reprinted from reference 16. Copyright 2020 American Chemical Society. (C) Potential-dependence of the local pH measured with SERS in the vicinity of a Cu GDE. Reprinted from reference 54. Copyright 2021 American Chemical Society. (D) Faradaic efficiencies during CO₂ reduction under a potentiostatic applied potential of -0.7 V vs RHE (first column) and during application of alternating voltage steps between -0.7 V and an anodic voltage, $E_{\rm an}$, in the range 0.6 to 1.5 V. Pulse duration: 1 s. Reprinted from reference 56. Copyright 2021 American Chemical Society.

this enhancement to irreversible morphological changes of the Cu surface during the oxidation/reduction cycles. For pulse sequences with $E_{\rm an} \geq 1.0$ V, Roldan Cuenya and co-workers observed a substantial increase in the Faradaic efficiency of methane (Figure 2D). SERS suggests the depletion of surface hydroxide and an increase in Cu₂O with increasing $E_{\rm an}$. On the basis of these observation and other corroborating evidence, they suggested that the periodic formation of Cu₂O lowers the local pH, which promotes the formation of methane during the cathodic segments of the pulse sequence.

Proton Donor/Acceptor Identity

So far, we have not considered the identity of the proton donor (or acceptor) in reactions like reaction 1. The chemical properties of the proton donor/acceptor can affect the thermodynamics and kinetics of multi-proton/electron transfer reactions. ^{2,18,19,57,58} In the following, we will give several recent illustrative examples of how changes in proton donor can accelerate the HER and modulate its mechanism.

Bren and co-workers reported a dependence of the mechanism of the HER catalyzed by a cobalt porphyrin peptide in aqueous solution on the pK_a of the buffer acid.⁵⁸ Briefly, they found that the peak current due to the HER during a CV monotonically increases with decreasing pK_a of the buffer acid at a constant pH of 5.2. Further, they found that the halfwave potential of the current wave due to the HER in the CV is independent of pK_a for pK_a values >7.4, whereas it shifts to more positive values with decreasing pK_a for pK_a values <7.4 (Figure 3A). On the basis of these observations and additional analysis of their CVs, Bren and co-workers proposed that for buffer acids with pK_a values >7.4, the half-wave potential is determined by the potential of the Co(II)/Co(I) redox couple, and the protonation of the Co(III)—H species is rate-determining (Figure 3B, right pathway). By contrast, in the presence of buffer acids with pK_a values <7.4, Co(I) is quickly converted to Co(III)-H. This conversion is sufficiently fast to deplete the available buffer acid in the diffusion layer of the electrode, thereby permitting the observation of HER activity at potentials above the formal Co(II)/Co(I) reduction potential. The protonation of the Co(II)-H species is presumed the rate-determining step in this mechanism (Figure 3B, left pathway). This study demonstrates that a change in the proton donor/acceptor may not only affect the rate of a reaction but also its pathway.

Glass, Pyun, Lichtenberger, and co-workers explored the effects of buffer composition on the HER catalyzed by a homogeneous [2Fe-2S]-metallopolymer electrocatalyst and a polycrystalline Pt electrode. ¹⁹ Specifically, they contrasted the rates of the HER in pH-neutral solutions of the chloride salt of tris(hydroxymethyl)aminomethane (TRIS- H^{+} Cl⁻; pK_a of TRIS-H⁺ 8.1) with those in pH-neutral solutions of sodium phosphate $Na^{+}(H_{2}PO_{4}^{-})$ (pK_a of $H_{2}PO_{4}^{-}$ 6.5). By characterizing the HER activity of the [2Fe-2S]metallopolymer electrocatalyst, they found that the peak HER current is enhanced by a factor of 70 in the presence of [TRIS-H⁺]Cl⁻ compared to that in $Na^+(H_2PO_4^-)$ buffer. They attributed the rate enhancement to a combination of factors, including the high degree of protonation of TRIS at pH 7 (due to its higher p K_a compared to that of $H_2PO_4^-$), the positive charge of TRIS-H⁺ (as opposed to $H_2PO_4^-$, which is depleted in the electrochemical double layer when the electrode is cathodically polarized), and a complex interplay between the [2Fe-2S]-metallopolymer electrocatalyst and Na⁺, which affects the catalyst's diffusion properties in solution and its ability to adsorb on the glassy carbon electrode. While the rate of the HER is enhanced upon switching from Na⁺(H₂PO₄⁻) to [TRIS-H⁺]Cl⁻ buffer, the half-wave potential is not significantly altered and is determined by the redox potential of the [2Fe-2S]-metallopolymer electrocatalyst. By contrast, on a Pt electrode, the HER current shifts by about 92 mV in the anodic direction in the presence of phosphate (Figure 3C). They attributed this shift to the decrease in the thermodynamic poten-

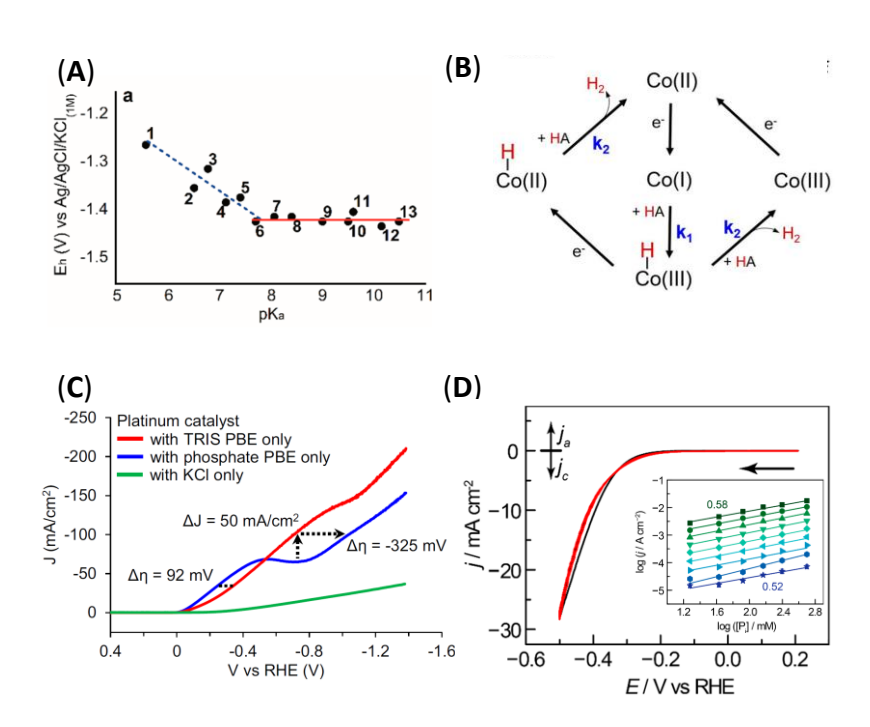


Figure 3: (A) Half-wave potential of the HER as a function of pK_a of the proton donor (pH 5.2 for all solutions). Reprinted from reference 58. Copyright 2020 American Chemical Society. (B) Proposed switch of the HER mechanism with pK_a of the buffer acid (left: pK_a \leq 7.4; right: pK_a >7.4). Adapted from reference 58. Copyright 2020 American Chemical Society. (C) Dependence of the HER current density on a polycrystalline Pt rotation disk electrode on $U_{\rm RHE}$ in 1 M [TRIS-H⁺]Cl⁻ (red), 0.75 M Na⁺(H₂PO₄⁻) (blue), and 0.1 M KCl (black) at a bulk pH of 7.00±0.01. The black dashed lines and arrows indicate the differences in overpotential and current density at select points. Reprinted from reference 19. Copyright 2020 Clary et al. (D) CV of a polycrystalline Au electrode in contact with an aqueous electrolyte containing 0.1 M HClO₄ and 1.0 M NaClO₄ at pH 1 (black) and 2.8 M potassium phosphate buffer at pH 6.8 (red). Inset: Logarithm of HER current density as a function of phosphate concentration of an aqueous electrolyte (pH = 6.1) containing 1.0 M NaClO₄ at overpotentials ranging from 0.1 V (dark blue) to 0.5 V (dark green). The numbers indicate extracted reaction orders in phosphate. Reprinted from reference 18. Copyright 2019 American Chemical Society.

tial requirement for HER upon changing the primary proton donor from TRIS-H⁺ (pK_a 8.1) to $\rm H_2PO_4^-$ (pK_a 6.5). At more negative potentials, phosphate is depleted, and the current becomes diffusion limited until the potential is sufficiently negative for direct $\rm H_2O$ reduction. By contrast, in [TRIS-H⁺]Cl⁻ buffer, the current is maintained because of the high population of the protonated state of TRIS at pH 7. Only at \sim 150 mA cm⁻² does the current become diffusion limited.

Surendranath and co-workers presented a detailed mechanistic analysis on the effects of the proton donor on the rate of the HER on Au electrodes. 18 They found that the rate of the HER in saturated potassium phosphate at nearneutral pH is virtually equal to the rate of the reaction at pH 1 (on the RHE scale) (Figure 3D). They found a reaction order of 0.6 in phosphate (inset, Figure 3D). They determined that a simple model assuming direct competition of phosphate in solution with water and hydronium ions as proton donors in the HER is inconsistent with the experimentally observed fractional order. Surendranath and co-workers suggested that the interaction of cations with phosphate species in the electrochemical double layer plays a critical role in mediating the promotion of the HER. By contrast, they demonstrated that borate does not act as a proton donor for the HER on Au. On the basis of these findings, they speculated that the different strengths of ion-pairing interactions in the two electrolytes to be responsible for their different impact on the rate of the HER. This work¹⁸ and the study by Glass, Pyun, Lichtenberger, and co-workers 19 highlight that the effects of a donor/acceptor species in solution are a complex function of a multitude of factors, including ion-pairing effects, interactions of the electrolyte species with the catalyst, the donor/acceptor species' charge state under the prevailing conditions, and the desired operating potential/current.

It is important to recognize that the primary donor species can also change with the pH of the solution. For example, using DFT calculations and microkinetic modeling, Chan and coworkers determined that the experimentally observed polarization curves for HER on Pt electrodes can be well described by a switch in the proton donor from hydronium to water with increasing pH.² Because the abstraction of a proton from water is associated with a higher activation barrier than that from hydronium, the reaction proceeds more slowly in alkaline media. Further, in an intermediate pH regime (2-4), Chan and co-workers observed a potential-induced switch between the two mechanistic regimes: At low overpotential, hydronium is the proton donor. However, with increasing overpotential, hydronium is depleted, and water becomes the primary donor.

Nernstian Shifts and Proton Delivery Rate

During current flow, a concentration gradient of electrolytic and reacting species within the boundary layer of the electrode may exist, resulting in a deviation of the near-electrode concentrations from their bulk values (for example, see Figure 2C). 20-25 If protons are consumed or produced during the electrocatalytic process at a rate that alters the pH in the boundary layer, the overpotential of the reaction will be altered because the equilibrium potential (Nernstian potential) will shift by an amount $\Delta\phi_{\text{Nernst}}$. We can identify two distinct contributions to $\Delta\phi_{\text{Nernst}}$: 20 (1) An increase in the local pH by one unit will result in a 60 mV negative shift: $\Delta \phi_{\rm pH} = 0.06 \, \rm V \times (p H_{\rm bulk} - p H_{\rm local})$ (assuming an equal number of protons and electrons are transferred in the process). (2) If the change in pH alters the concentration of a reactant, an additional negative shift of 60/nmV, where n is the number of electrons transferred in the reaction, per one order of magnitude decrease in the concentration results: $\Delta\phi_{\rm conc} = \frac{0.06\,\mathrm{V}}{n} \times \log(\frac{c_{\rm local}}{c_{\rm bulk}})$, where $c_{\rm bulk}$ and $c_{\rm local}$ refer to the concentrations of the species in the bulk and at the surface, respectively.

The measurement of local pH values under reaction conditions has only been carried out in recent years: Employing SEIRAS, Smith and co-workers quantified the pH within a 5-10 nm thin electrolyte layer of sputtered Cu electrodes

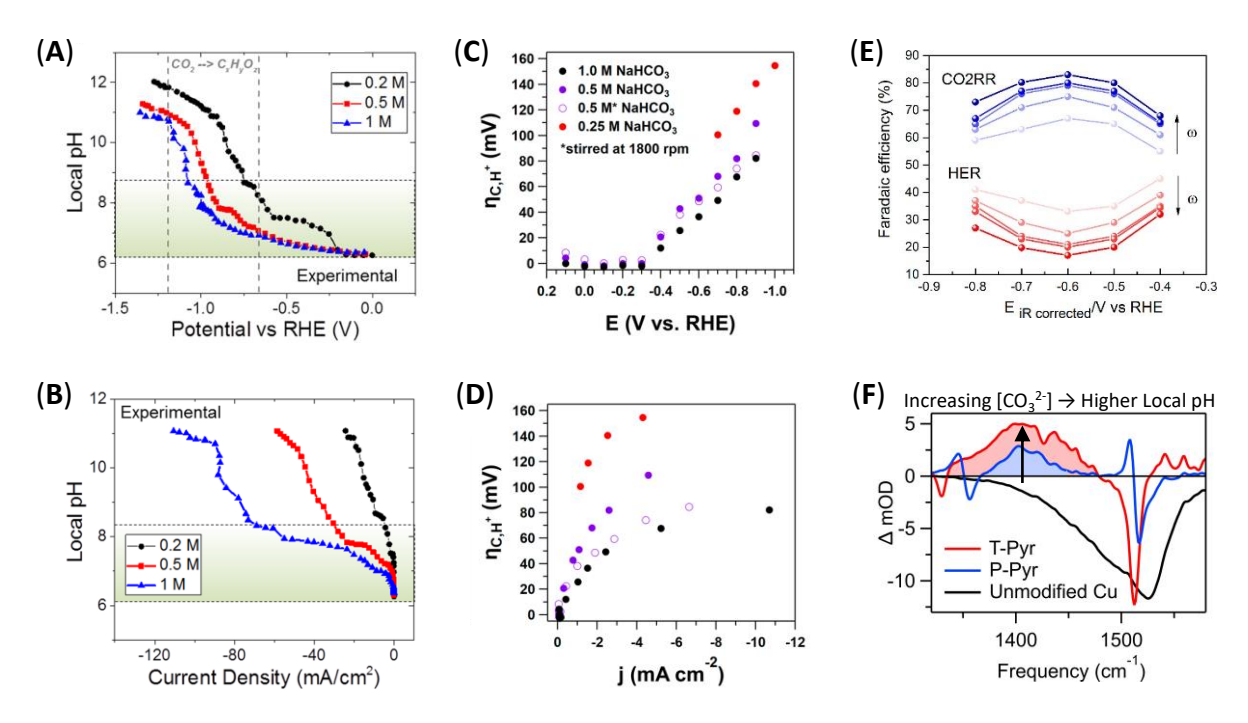


Figure 4: (A, B) Dependence of the local pH on $U_{\rm RHE}$ and measured current density. The local pH was measured within 5-10 nm of a sputtered Cu electrode in CO₂-saturated phosphate buffer at near-neutral bulk pH at the indicated concentrations. Reprinted from reference 22. Copyright 2019 American Chemical Society. (C, D) Dependence of the concentration overpotential of CO₂-to-CO reduction on $U_{\rm RHE}$ and measured current density. The measurements are for a rough Au electrode in contact with CO₂-saturated bicarbonate buffer at near-neutral bulk pH. Reprinted from reference 59. Copyright 2018 American Chemical Society. (E) Dependence of the Faradaic efficiencies for the products of HER and CO₂-to-CO conversion (CO₂RR) on the rotation rate (ω) of an RDE. Rotation rate range: 800 to 2500 rpm. Reprinted from reference 60. Copyright 2020 American Chemical Society. (F) Spectra taken at -1.5 V vs Ag/AgCl showing the accumulation of carbonate at 1410 cm⁻¹ (shaded area) during CO₂ reduction on unmodified Cu and in the presence of electrodeposited organic films derived from 1-(4-toly)pyridinium (T-Pyr) and 1-(4-pyridyl)pyridinium (P-Pyr). Data from reference 61. Copyright 2019 American Chemical Society.

in phosphate-buffered electrolyte during CO₂ reduction at current densities from a few to several tens of mA cm⁻². ²² The technique is based on the measurement of the relative integrated band areas of the distinct bands of the anions of phosphoric acid in the vicinity of the electrode. Their key findings are as follows: (1) For a given applied potential, the magnitude of the local pH increase is similar for 0.5 and 1.0 M phosphate buffers because the increased buffer capacity is offset by an acceleration of the HER with increasing phosphate concentration (Figure 4A). (2) In a 0.2 M phosphate buffer, the local pH steeply increases with absolute current density; it is about 5 pH units higher than the bulk pH at a cathodic current density of $\sim 20 \text{ mA cm}^{-2}$ (Figure 4B). Increasing the buffer capacity to 0.5 or 1.0 M shifts the increase of the local pH to larger absolute current densities. (3) The increase in local pH results in a decrease in the local CO₂ concentration to a level of about 20% of its bulk value at an applied potential of -1.0V versus RHE.

It is important to note that the results of Smith and co-workers were obtained for an electrolyte that was not actively stirred or flown over the electrode (CO₂ bubbling and gas formation at the electrode were the only forms of electrolyte agitation in this study). Xu and co-workers explored the effects of electrolyte stirring on the concentration overpotential, defined as the increased overpotential resulting from changes in near-electrode concentrations of reacting species relative to those in the bulk. Using SEIRAS, they quantified the concentration overpotential due to local pH increase and CO₂ depletion during the reduction of CO₂ to CO on polycrystalline Au electrodes in contact with bicarbonate-buffered electrolyte. ⁵⁹ Their key findings are as follows: (1) The concentration overpotential at a given applied electrode potential decreases with increasing buffer capacity (Figure 4C). For example, at an applied potential of -0.9 V versus RHE, the concentration overpotential in 0.25 M bicarbonate is 141 mV, whereas it is only 82 mV in 1.0 M bicarbonate. This observation suggests that the increased buffer capacity effectively counters current-driven changes in the interfacial

concentrations. (2) Stirring the electrolyte can significantly decrease the concentration overpotential (Figure 4C, D). For example, at an applied electrode potential of -0.9 V, the concentration overpotential is 109 mV in the absence of stirring, whereas it is only 84 mV when the electrolyte is stirred. (3) SEIRAS measurements show that the near-surface concentration of CO₂ drops to near zero in the absence of stirring as the potential is changed from 0 to -0.9V versus RHE. By contrast, in a stirred electrolyte, the bulk CO₂ concentration is maintained even at -0.9 V, despite the higher local pH. This observation indicates that, under these conditions, the transport of CO_2 to the electrode is faster than its conversion to bicarbonate.

When we view the studies by Xu and coworkers and Smith and co-workers collectively, ^{22,59} we draw the following conclusions: (1) Effective convection (such as by stirring or flowing the electrolyte) is a straightforward and effective means for mitigating concentration overpotentials. (2) Increasing the buffer capacity can be a suitable means for minimizing overpotentials. However, the degree of success of this strategy sensitively depends on the properties of the chosen buffer system: pH buffers can directly engage as proton donors/acceptors in the interfacial electrocatalytic processes, most notably in the HER. The promotion of the HER leads to faster consumption of interfacial protons, thereby opposing the effect of increased buffer capacity, as observed by Smith and coworkers. 22 (3) The simulated near-surface concentrations by Smith and co-workers exhibit semi-quantitative agreement with their experimentally measured concentrations. This agreement suggests that mass-transport models are an important tool in the prediction of concentration overpotentials. $^{20-25}$

The understanding of concentration overpotentials has both fundamental and practical significance. As shown by Xu and coworkers, ⁵⁹ their measured concentration overpotentials can significantly affect electrokinetic parameters, such as Tafel slopes and reaction orders. Therefore, for fundamental studies on electrokinetics, it is essential that concentration

overpotentials are minimized or corrected for if significant overpotentials cannot be avoided. In this regard, it is critical to measure the local pH under reaction conditions. Apart from SERS and SEIRAS, a variety of other tools can be used to probe the local pH. Alternative methods include the use of scanning probe microscopy, ^{62,63} rotating ring disk electrodes, ^{64,65} nonfaradaic reactions, ⁴⁷ and fluorescence spectroscopy. ⁶⁶ These and other techniques were recently reviewed. ⁶⁷

Low overpotential and high reaction selectivity are important goals in electrocatalysis, but they may not be necessarily achievable simultaneously. In practical systems, it may be necessary to tolerate a certain concentration overpotential to achieve a desired degree of selectivity. The chosen buffer system and mass transport conditions to the electrode surface can both greatly affect reaction selectivity. For example, Surendranath and co-workers reported that the promotion of the HER on polycrystalline Au by bicarbonate will lower the reaction selectivity for CO₂-to-CO conversion.⁶⁸ For these reasons, it is essential to evaluate the impact of the electrolyte buffer system on the intrinsic rates of the desired and undesired reactions at a given electrocatalytic interface. A possible strategy to quantify these impacts is to measure the rate of the HER as a function of buffer capacity and compositions. For example, Surendranath and co-workers showed that under mildly acidic conditions, phosphate species can compete with water as proton donors for the HER on Au electrodes, whereas borate species cannot. 18 A suitable buffer system should be determined on the basis of such experiments and other known properties of the catalytic system of interest.

It is important to note that hydrated alkali metal cations of the supporting electrolyte can also influence the local pH. Bell and co-workers demonstrated significant changes in the product spectrum of CO₂ reduction on Cu and Ag electrodes with the identity of the alkali metal cation of the supporting electrolyte. ⁶⁹ Using theoretical modeling, they proposed that the changes arise from the different pH buffer abilities of the hydrated alkali metal cations. Recently, this theoretical prediction was confirmed

by Cuesta and co-workers using SEIRAS⁷⁰ and Co and co-workers using a rotating ring disk electrode to probe the local pH.⁶⁵

Tuning the mass transport of protons and other reactants to the electrode surface can also be utilized to steer reaction selectivity. example, Koper and co-workers demonstrated that the competition between HER and CO₂to-CO conversion on polycrystalline Au electrodes in contact with CO₂-saturated 0.1 M NaHCO₃ can be controlled by modulation of the local pH. ⁶⁰ They showed that the Faradaic efficiency for CO_2 reduction at $U_{RHE} = -0.6$ V increases from 67% to 83% when the rotation rate of an RDE is increased from 800 to 2500 rpm (Figure 4E). They found that the increase in Faradaic efficiency is primarily a result of the suppression of the HER with increasing rotation rate. The increased rotation rate improves the mass transport of protons to the surface, thereby maintaining a low local pH, which leads to slower HER kinetics (on Au, they found that the rate of water reduction increases with increasing alkalinity in the pH range 10-13).

In a more recent article, Koper and coworkers investigated the competition between HER and CO₂-to-CO conversion under mildly acidic conditions. ⁷¹ They determined that the reduction of protons can be completely suppressed if the rate of CO formation is equal to or exceeds the rate of proton transport to the electrode. Under these conditions, hydroxide ions that are formed during CO₂-to-CO and H₂O reduction neutralize protons that arrive at the surface before they can be reduced to hydrogen. If the rate of hydroxide formation is too high, a significant fraction of CO₂ reacts with hydroxide to bicarbonate.

Bell and co-workers showed that pulsed electrolysis can be utilized to enhance the production of C2+ hydrocarbon products during CO₂ reduction on Cu electrodes. ^{25,72} On the basis of a time-dependent continuum model, they revealed that the desirable product spectrum (in comparison with constant-potential electrolysis) is a result a periodically high local pH, CO₂ concentration, and overpotential during the pulse sequences. ²⁵

The local pH and/or the transport of pro-

tons to the surface can also be controlled by modifying the electrode surface. For example, we assessed the relative local pH on Cu electrodes modified with organic films derived from N-substituted arylpyridinium derivatives and immersed in CO_2 -saturated 0.5 M KHCO₃. ⁶¹ By monitoring the infrared band of carbonate at 1410 cm^{-1} with SEIRAS, we quantified the accumulation of carbonate at the electrode/electrolyte interface (Figure 4F). We found that the degree of carbonate accumulation is most pronounced at the interface involving films derived from 1-(4-toly)pyridinium (T-Pvr), whereas less carbonate accumulates at interfaces involving films derived from 1-(4pyridyl)pyridinium (P-Pyr). No significant accumulation of this species occurs at the unmodified interface. As carbonate is formed by the reaction of hydroxide with bicarbonate, an increase in the carbonate band suggests an increase in local pH. As a high local pH tends to favor C2+ products, our findings provide a rationale for an earlier observation by Peters, Agapie and co-workers, ⁷³ who reported that T-Pyr-modified electrodes exhibit a high selectivity for C2+ hydrocarbons. Recently, Agapie, Peters, and co-workers demonstrated that the rate of proton diffusion can be tuned by related organic films. ⁷⁴ Local pH effects in various highsurface area electrodes have been suggested to play a key role in modulating reaction selectivitv. ^{21,75}

An elegant way of controlling the rate of proton transport based on lipid-modified selfassembled monolayers (SAMs) was reported by Barile and co-workers. ⁷⁶ Building on earlier work by Gewirth and co-workers, 77 they used thiol-based SAMs to link a molecular ORR catalyst to an Au electrode and blanketed the assembly with a lipid membrane. By adjusting the length of the SAM linkers, they controlled the distance between electrode and catalyst, which provides control over the electrontransfer rate. Adjustment of the concentration of proton carriers in the membrane provides control over the rate of proton delivery to the catalyst. Barile and co-workers demonstrated that they can modify the rate of the ORR over a wide range by independently tuning the relative rates of electron and proton transfer. Interestingly, changing the concentration of proton carrier in the lipid does not result in a significant Nernstian shift, but affects the rate of the ORR. This result suggest that the platform permits the selective tuning of the kinetics of the reaction without significantly altering its thermodynamics.

GDEs are of great practical significance for CO₂ reduction. ^{54,56,78,79} The first studies of the local pH at GDE/electrolyte interfaces have just recently appeared. GDEs in contact with highly alkaline electrolytes have been found particularly effective for the production of desirable products with high selectivity and at low overpotentials. As CO₂ reacts with OH⁻ to bicarbonate under these conditions, a pH gradient is expected to form at the electrolyte/electrode interface.

By monitoring the relative integrated areas of the characteristic Raman bands of carbonate and bicarbonate, Francisco, Wang, and coworkers mapped the pH gradient over a distance of several tens of micrometers from a GDE into the electrolyte (1 M KOH) under continuousflow CO₂ reduction.⁷⁹ They found that the pH within a distance of $\sim 10 \ \mu \text{m}$ of the GDE is significantly lower than that of the bulk electrolyte and increases with increasing current density $(pH\sim9 \text{ at } 50 \text{ mA cm}^{-2} \text{ and } pH\sim10 \text{ at } 100 \text{ mA}$ cm^{-2}). Further, the pH increases by 1-2 pH units over a distance of several tens of μm , depending on the current density and electrolyteand CO₂-flow conditions. These results indicate that the homogeneous reaction between CO₂ with OH⁻ causes a decrease in the local pH and that reduction of CO₂ counters this effect through the production of hydroxide. Francisco, Wang, and co-workers suggested this pH gradient as the cause of lower absolute overpotential requirements for the reduction of CO₂ in alkaline electrolyzers.

Using SERS, Kenis, Gewirth, and co-workers estimated the pH within a ~ 3 nm layer of a Cu GDE electrode under CO₂ reduction conditions in 1 M KOH to be >11 (after virtually complete reduction of all Cu oxide phases). ⁵⁴ The different findings in the two studies likely originate from different cell geometries and flow

conditions. These pioneering studies demonstrate the utility of Raman spectroscopy for measuring the local pH on micro- and nanometer length scales. This technique has the potential to inform the design of GDEs and choice of reaction conditions for optimal electrolyzer performance.

Controlling the distribution of surface concentrations across the porous catalytic layer of a GDE is essential for the generation of desirable product distributions. For example, Sargent and co-workers recently showed how the electrolyte pH can be used to tune the product selectivity at a GDE.⁸⁰ In 1 M KOH electrolyte, the penetration depth of CO₂ into the electrolyte/catalyst layer is on the order of a few microns. As a result, the catalytic layer is in contact with a low concentration of CO_2 , which is distributed over a wide penetration depth. By contrast, in highly alkaline electrolyte (10 M KOH), the penetration of CO_2 into the porous catalytic layer is limited to ~120 nm) by the neutralization reaction between CO₂ and OH⁻. The steep concentration gradient in 10 M KOH ensures that the catalyst is in contact with a relatively high concentration of CO_2 . The high concentration of CO₂ and spatially narrow distribution promotes C-C bond formation, yielding a 70% Faradaic efficiency for ethylene at a potential of -0.55 V versus RHE. Using DFT calculations, Sargent and co-workers identified additional promotion effects of OH⁻ that also contribute to the preferential formation of ethylene. Of course, this high Faradaic efficiency comes at the cost of irreversibly losing a significant amount of CO₂ to bicarbonate. In a more recent work, Sargent and co-workers achieved 77% single-pass CO₂ utilization by employing highly acidic electrolytes.⁸¹

Summary and Outlook

As illustrated by the examples in this Perspective, the pH can influence the rates, mechanisms, and selectivity of electrocatalytic multiproton/electron transfer processes in a multitude of ways. Elucidating these pathways is of practical and fundamental significance. The

studies highlighted in this Perspective provide examples of pH-dependent properties of the interface that should be considered and how these properties can be probed: (1) The adsorption energies and site preferences of a number of intermediates that feature in the mechanisms of ORR, HER, and CO/CO₂ reduction exhibit a dependence on pH. In future theoretical and experimental investigations of electrocatalytic processes, this possibility and its effect on mechanisms and rates should be considered. (2) During electrolysis at near-neutral bulk pH, the local pH can significantly deviate from the bulk pH. It is advisable to evaluate the local pH under the relevant operating conditions. To determine the local pH and concentration overpotentials, Raman and IR spectroscopy have emerged as powerful tools. Alternative methods for this purpose were reviewed recently. ⁶⁷ A deeper understanding of pH gradients in complex environments, such as in GDEs, will help guide the design of electrolyzer cells and catalyst morphology and the choice of reaction conditions. Modeling of mass transport effects is another effective strategy for estimating the local pH. (3) Surface speciation may significantly change with pH. Raman, IR, and x-ray spectroscopies can also probe the prevalent oxide phases and changes in site preference of intermediates. However, correlating surface speciation with catalysis remains challenging. Performing spectroscopy under conditions as closely as possible to those during catalysis minimizes the chance of possible misinterpretations. (4) The identity and concentration of proton donors/acceptors can profoundly impact the rates of some electrocatalytic reactions. To optimize catalytic performance, the impact of a given donor/acceptor on the various competing reactions should be systematically investigated in electrokinetic experiments.

Biographies

Vincent J. Ovalle earned his B.Sc. degree in Chemistry from Loyola Marymount University in Los Angeles, California, in 2016. Currently, he is a Ph.D. student in Prof. Matthias Waegele's research team at Boston College. His research focuses on operando spectroscopic characterization of electrocatalytic interfaces.

Matthias M. Waegele received his B.S. degree in Chemistry (2006) from the Technical University Munich and Ph.D. degree in Chemistry from the University of Pennsylvania (2011) working with Prof. Feng Gai. Following his postdoctoral work under the direction of Prof. Tanja Cuk at the University of California, Berkeley, he assumed his current position of Assistant Professor of Chemistry at Boston College in 2015. His research team engages in spectroscopic investigation of catalytic interfaces that show potential for the synthesis of renewable fuels and high-value commodity chemicals.

Acknowledgement This work was supported by a CAREER award from the National Science Foundation (Award No.: CHE-1847841). We thank Professor Karen Chan and Professor Junwei (Lucas) Bao for helpful discussions about electric field effects.

References

- (1) Dubouis, N.; Grimaud, A. The Hydrogen Evolution Reaction: from Material to Interfacial Descriptors. *Chem. Sci.* **2019**, *10*, 9165–9181.
- (2) Lamoureux, P. S.; Singh, A. R.; Chan, K. pH Effects on Hydrogen Evolution and Oxidation over Pt(111): Insights from First-Principles. *ACS Catal.* **2019**, *9*, 6194–6201.
- (3) Li, M. F.; Liao, L. W.; Yuan, D. F.; Mei, D.; Chen, Y.-X. pH Effect on Oxygen Reduction Reaction at Pt(111) Electrode. *Electrochim. Acta* **2013**, *110*, 780–789.
- (4) Gewirth, A. A.; Varnell, J. A.; Di-Ascro, A. M. Nonprecious Metal Catalysts for Oxygen Reduction in Heterogeneous Aqueous Systems. *Chem. Rev.* **2018**, *118*, 2313–2339.
- (5) Lee, C. H.; Kanan, M. W. Controlling H⁺

- vs CO₂ Reduction Selectivity on Pb Electrodes. ACS Catal. **2015**, 5, 465–469.
- (6) Nitopi, S.; Bertheussen, E.; Scott, S. B.; Liu, X.; Engstfeld, A. K.; Horch, S.; Seger, B.; Stephens, I. E. L.; Chan, K.; Hahn, C. et al. Progress and Perspectives of Electrochemical CO₂ Reduction on Copper in Aqueous Electrolyte. *Chem. Rev.* 2019, 119, 7610–7672.
- (7) Siddharth, K.; Chan, Y.; Wang, L.; Shao, M. Ammonia Electro-Oxidation Reaction: Recent Development in Mechanistic Understanding and Electrocatalyst Design. Curr. Opin. Electrochem. 2018, 9, 151–157.
- (8) Wallace, S. W.; McCrum, I. T.; Janik, M. J. Ammonia Electro-Oxidation Mechanism on the Platinum (100) Surface. *Catal. Today* **2021**, *371*, 50–57.
- (9) Herrero, E.; Feliu, J. M. Understanding Formic Acid Oxidation Mechanism on Platinum Single Crystal Electrodes. Curr. Opin. Electrochem. 2018, 9, 145–150.
- (10) Zhang, M.-K.; Chen, W.; Wei, Z.; Xu, M.-L.; He, Z.; Cai, J.; Chen, Y.-X.; Santos, E. Mechanistic Implication of the pH Effect and H/D Kinetic Isotope Effect on HCOOH/HCOO⁻ Oxidation at Pt Electrodes: A Study by Computer Simulation. ACS Catal. 2021, 11, 6920–6930.
- (11) Lang, C.; Li, J.; Yang, K. R.; Wang, Y.; He, D.; Thorne, J. E.; Croslow, S.; Dong, Q.; Zhao, Y.; Prostko, G. et al. Observation of a Potential-Dependent Switch of Water-Oxidation Mechanism on Co-Oxide-Based Catalysts. *Chem* **2021**,
- (12) Yang, X.; Wang, Y.; Li, C. M.; Wang, D. Mechanisms of Water Oxidation on Heterogeneous Catalyst Surfaces. *Nano Res.* 2021, DOI: 10.1007/s12274-021-3607-5.
- (13) Koper, M. T. M. Theory of Multiple Proton-Electron Transfer Reactions and Its Implications for Electrocatalysis. *Chem. Sci.* **2013**, *4*, 2710–2723.

- (14) Duan, Z.; Henkelman, G. Theoretical Resolution of the Exceptional Oxygen Reduction Activity of Au(100) in Alkaline Media. ACS Catal. 2019, 9, 5567–5573.
- (15) Kelly, S. R.; Kirk, C.; Chan, K.; Nørskov, J. K. Electric Field Effects in Oxygen Reduction Kinetics: Rationalizing pH Dependence at the Pt(111), Au(111), and Au(100) Electrodes. J. Phys. Chem. C 2020, 124, 14581–14591.
- (16) Yang, S.; Hetterscheid, D. G. H. Redefinition of the Active Species and the Mechanism of the Oxygen Evolution Reaction on Gold Oxide. ACS Catal. 2020, 10, 12582–12589.
- (17) Weitzner, S. E.; Akhade, S. A.; Varley, J. B.; Wood, B. C.; Otani, M.; Baker, S. E.; Duoss, E. B. Toward Engineering of Solution Microenvironments for the CO₂ Reduction Reaction: Unraveling pH and Voltage Effects from a Combined Density-Functional-Continuum Theory. J. Phys. Chem. Lett. 2020, 11, 4113-4118.
- (18) Jackson, M. N.; Jung, O.; Lamotte, H. C.; Surendranath, Y. Donor-Dependent Promotion of Interfacial Proton-Coupled Electron Transfer in Aqueous Electrocatalysis. ACS Catal. 2019, 9, 3737–3743.
- (19) Clary, K. E.; Karayilan, M.; McCleary-Petersen, K. C.; Petersen, H. A.; Glass, R. S.; Pyun, J.; Lichtenberger, D. L. Increasing the Rate of the Hydrogen Evolution Reaction in Neutral Water with Protic Buffer Electrolytes. Proc. Natl. Acad. Sci. U. S. A. 2020, 117, 32947–32953.
- (20) Singh, M. R.; Clark, E. L.; Bell, A. T. Effects of Electrolyte, Catalyst, and Membrane Composition and Operating Conditions on the Performance of Solar-Driven Electrochemical Reduction of Carbon Dioxide. *Phys. Chem. Chem. Phys.* 2015, 17, 18924–18936.

- (21) Raciti, D.; Mao, M.; Park, J. H.; Wang, C. Local pH Effect in the CO₂ Reduction Reaction on High-Surface-Area Copper Electrocatalysts. J. Electrochem. Soc. 2018, 165, F799–F804.
- (22) Yang, K.; Kas, R.; Smith, W. A. In Situ Infrared Spectroscopy Reveals Persistent Alkalinity near Electrode Surfaces during CO₂ Electroreduction. J. Am. Chem. Soc. 2019, 141, 15891–15900.
- (23) Dau, H.; Pasquini, C. Modelling the (Essential) Role of Proton Transport by Electrolyte Bases for Electrochemical Water Oxidation at Near-Neutral pH. *Inorganics* **2019**, 7, 20.
- (24) Zhang, M.-K.; Chen, W.; Xu, M.-L.; Wei, Z.; Zhou, D.; Cai, J.; Chen, Y.-X. How Buffers Resist Electrochemical Reaction-Induced pH Shift under a Rotating Disk Electrode Configuration. *Anal. Chem.* 2021, 93, 1976–1983.
- (25) Bui, J. C.; Kim, C.; Weber, A. Z.; Bell, A. T. Dynamic Boundary Layer Simulation of Pulsed CO₂ Electrolysis on a Copper Catalyst. ACS Energy Lett. 2021, 6, 1181–1188.
- (26) Boulatov, R.; Collman, J. P.; Shiryaeva, I. M.; Sunderland, C. J. Functional Analogues of the Dioxygen Reduction Site in Cytochrome Oxidase: Mechanistic Aspects and Possible Effects of Cu_B. J. Am. Chem. Soc. 2002, 124, 11923–11935.
- (27) Huynh, M. H. V.; Meyer, T. J. Proton-Coupled Electron Transfer. *Chem. Rev.* **2007**, *107*, 5004–5064.
- (28) Irebo, T.; Reece, S. Y.; Sjödin, M.; Nocera, D. G.; Hammarström, L. Proton-Coupled Electron Transfer of Tyrosine Oxidation: Buffer Dependence and Parallel Mechanisms. J. Am. Chem. Soc. 2007, 129, 15462–15464.
- (29) Gerken, J. B.; McAlpin, J. G.; Chen, J. Y. C.; Rigsby, M. L.; Casey, W. H.;

- Britt, R. D.; Stahl, S. S. Electrochemical Water Oxidation with Cobalt-Based Electrocatalysts from pH 0–14: The Thermodynamic Basis for Catalyst Structure, Stability, and Activity. J. Am. Chem. Soc. **2011**, 133, 14431–14442.
- (30) Takashima, T.; Hashimoto, K.; Nakamura, R. Mechanisms of pH-Dependent Activity for Water Oxidation to Molecular Oxygen by MnO₂ Electrocatalysts. J. Am. Chem. Soc. 2012, 134, 1519–1527.
- (31) Kushner-Lenhoff, M. N.; Blakemore, J. D.; Schley, N. D.; Crabtree, R. H.; Brudvig, G. W. Effects of Aqueous Buffers on Electrocatalytic Water Oxidation with an Iridium Oxide Material Electrodeposited in Thin Layers from an Organometallic Precursor. *Dalton Trans.* **2013**, 42, 3617–3622.
- (32) Chen, X.; Aschaffenburg, D. J.; Cuk, T. Selecting Between two Transition States by Which Water Oxidation Intermediates Decay on an Oxide Surface. *Nat. Catal.* **2019**, *2*, 820–827.
- (33) Yeh, K.-Y.; Janik, M. J. Density Functional Theory-Based Electrochemical Models for the Oxygen Reduction Reaction: Comparison of Modeling Approaches for Electric Field and Solvent Effects. *J. Comp. Chem.* **2011**, *32*, 3399–3408.
- (34) Zhu, S.; Qin, X.; Yao, Y.; Shao, M. pH-Dependent Hydrogen and Water Binding Energies on Platinum Surfaces as Directly Probed through Surface-Enhanced Infrared Absorption Spectroscopy. J. Am. Chem. Soc. 2020, 142, 8748–8754.
- (35) Liu, X.; Schlexer, P.; Xiao, J.; Ji, Y.; Wang, L.; Sandberg, R. B.; Tang, M.; Brown, K. S.; Peng, H.; Ringe, S. et al. pH Effects on the Electrochemical Reduction of CO₍₂₎ Towards C₂ Products on Stepped Copper. *Nat. Commun.* **2019**, *10*, 32.
- (36) Ringe, S.; Morales-Guio, C. G.; Chen, L. D.; Fields, M.; Jaramillo, T. F.;

- Hahn, C.; Chan, K. Double Layer Charging Driven Carbon Dioxide Adsorption Limits the Rate of Electrochemical Carbon Dioxide Reduction on Gold. *Nat. Commun.* **2020**, *11*, 33.
- (37) Chan, K. A Few Basic Concepts in Electrochemical Carbon Dioxide Reduction. *Nat. Commun.* **2020**, *11*, 5954.
- (38) Mills, J. N.; McCrum, I. T.; Janik, M. J. Alkali Cation Specific Adsorption onto fcc(111) Transition Metal Electrodes. Phys. Chem. Chem. Phys. 2014, 16, 13699–13707.
- (39) Waegele, M. M.; Gunathunge, C. M.; Li, J.; Li, X. How Cations Affect the Electric Double Layer and the Rates and Selectivity of Electrocatalytic Processes. J. Chem. Phys. 2019, 151, 160902.
- (40) McCrum, I. T.; Janik, M. J. pH and Alkali Cation Effects on the Pt Cyclic Voltammogram Explained Using Density Functional Theory. J. Phys. Chem. C 2016, 120, 457–471.
- (41) Chen, X.; McCrum, I. T.; Schwarz, K. A.; Janik, M. J.; Koper, M. T. M. Coadsorption of Cations as the Cause of the Apparent pH Dependence of Hydrogen Adsorption on a Stepped Platinum Single-Crystal Electrode. Angew. Chem. Int. Ed. 2017, 56, 15025–15029.
- (42) Janik, M. J.; McCrum, I. T.; Koper, M. T. On the Presence of Surface Bound Hydroxyl Species on Polycrystalline Pt Electrodes in the "Hydrogen Potential Region" (0–0.4V-RHE). J. Catal. 2018, 367, 332–337.
- (43) Zheng, J.; Nash, J.; Xu, B.; Yan, Y. Perspective—Towards Establishing Apparent Hydrogen Binding Energy as the Descriptor for Hydrogen Oxidation/Evolution Reactions. J. Electrochem. Soc. 2018, 165, H27–H29.
- (44) Cheng, T.; Wang, L.; Merinov, B. V.; Goddard, W. A. Explanation of Dramatic

- pH-Dependence of Hydrogen Binding on Noble Metal Electrode: Greatly Weakened Water Adsorption at High pH. *J. Am. Chem. Soc.* **2018**, *140*, 7787–7790.
- (45) Yang, X.; Nash, J.; Oliveira, N.; Yan, Y.; Xu, B. Understanding the pH Dependence of Underpotential Deposited Hydrogen on Platinum. Angew. Chem. Int. Ed. 2019, 58, 17718–17723.
- (46) Ledezma-Yanez, I.; Wallace, W. D. Z.; Sebastián-Pascual, P.; Climent, V.; Feliu, J. M.; Koper, M. T. M. Interfacial Water Reorganization as a pH-Dependent Descriptor of the Hydrogen Evolution Rate on Platinum Electrodes. *Nat. Energy* **2017**, *2*, 17031.
- (47) Ryu, J.; Surendranath, Y. Tracking Electrical Fields at the Pt/H₂O Interface during Hydrogen Catalysis. J. Am. Chem. Soc. 2019, 141, 15524–15531.
- (48) Sorenson, S. A.; Patrow, J. G.; Dawlaty, J. M. Solvation Reaction Field at the Interface Measured by Vibrational Sum Frequency Generation Spectroscopy. J. Am. Chem. Soc. 2017, 139, 2369–2378.
- (49) Clark, M. L.; Ge, A.; Videla, P. E.; Rudshteyn, B.; Miller, C. J.; Song, J.; Batista, V. S.; Lian, T.; Kubiak, C. P. CO₂ Reduction Catalysts on Gold Electrode Surfaces Influenced by Large Electric Fields. J. Am. Chem. Soc. 2018, 140, 17643–17655.
- (50) Li, J.; Li, X.; Gunathunge, C. M.; Waegele, M. M. Hydrogen Bonding Steers the Product Selectivity of Electrocatalytic CO Reduction. *Proc. Nat. Acad. Sci. USA* 2019, 116, 9220–9229.
- (51) Gunathunge, C. M.; Ovalle, V. J.; Li, Y.; Janik, M. J.; Waegele, M. M. Existence of an Electrochemically Inert CO Population on Cu Electrodes in Alkaline pH. ACS Catal. 2018, 8, 7507–7516.

- (52) Chou, T.-C.; Chang, C.-C.; Yu, H.-L.; Yu, W.-Y.; Dong, C.-L.; Velasco-Vélez, J.-J.; Chuang, C.-H.; Chen, L.-C.; Lee, J.-F.; Chen, J.-M. et al. Controlling the Oxidation State of the Cu Electrode and Reaction Intermediates for Electrochemical CO₂ Reduction to Ethylene. *J. Am. Chem. Soc.* **2020**, *142*, 2857–2867.
- (53) Chang, X.; Zhao, Y.; Xu, B. pH Dependence of Cu Surface Speciation in the Electrochemical CO Reduction Reaction. ACS Catal. 2020, 10, 13737–13747.
- (54) Henckel, D. A.; Counihan, M. J.; Holmes, H. E.; Chen, X.; Nwabara, U. O.; Verma, S.; Rodríguez-López, J.; Kenis, P. J. A.; Gewirth, A. A. Potential Dependence of the Local pH in a CO₂ Reduction Electrolyzer. ACS Catal. 2021, 11, 255–263.
- (55) Kim, Y.-G.; Baricuatro, J. H.; Javier, A.; Gregoire, J. M.; Soriaga, M. P. The Evolution of the Polycrystalline Copper Surface, First to Cu(111) and Then to Cu(100), at a Fixed CO₂RR Potential: A Study by Operando EC-STM. Langmuir **2014**, 30, 15053–15056.
- (56) Jeon, H. S.; Timoshenko, J.; Rettenmaier, C.; Herzog, A.; Yoon, A.; Chee, S. W.; Oener, S.; Hejral, U.; Haase, F. T.; Roldan Cuenya, B. Selectivity Control of Cu Nanocrystals in a Gas-Fed Flow Cell through CO₂ Pulsed Electroreduction. J. Am. Chem. Soc. 2021, 143, 7578–7587.
- (57) Rountree, E. S.; Martin, D. J.; Mc-Carthy, B. D.; Dempsey, J. L. Linear Free Energy Relationships in the Hydrogen Evolution Reaction: Kinetic Analysis of a Cobaloxime Catalyst. *ACS Catal.* **2016**, *6*, 3326–3335.
- (58) Alvarez-Hernandez, J. L.; Sopchak, A. E.; Bren, K. L. Buffer pKa Impacts the Mechanism of Hydrogen Evolution Catalyzed by a Cobalt Porphyrin-Peptide. *Inorg. Chem.* **2020**, *59*, 8061–8069.

- (59) Dunwell, M.; Yang, X.; Setzler, B. P.; Anibal, J.; Yan, Y.; Xu, B. Examination of Near-Electrode Concentration Gradients and Kinetic Impacts on the Electrochemical Reduction of CO₂ using Surface-Enhanced Infrared Spectroscopy. ACS Catal. 2018, 8, 3999–4008.
- (60) Goyal, A.; Marcandalli, G.; Mints, V. A.; Koper, M. T. M. Competition between CO₂ Reduction and Hydrogen Evolution on a Gold Electrode under Well-Defined Mass Transport Conditions. J. Am. Chem. Soc. 2020, 142, 4154–4161.
- (61) Ovalle, V. J.; Waegele, M. M. Understanding the Impact of N-Arylpyridinium Ions on the Selectivity of CO₂ Reduction at the Cu/Electrolyte Interface. J. Phys. Chem. C 2019, 123, 24453–24460.
- (62) Filotás, D.; Fernández-Pérez, B. M.; Nagy, L.; Nagy, G.; Souto, R. M. Multi-Barrel Electrodes Containing an Internal Micro-Reference for the Improved Visualization of Galvanic Corrosion Processes in Magnesium-Based Materials using Potentiometric Scanning Electrochemical Microscopy. Sensor. Actuat. B: Chem. 2019, 296, 126625.
- (63) Monteiro, M. C. O.; Jacobse, L.; Touzalin, T.; Koper, M. T. M. Mediator-Free SECM for Probing the Diffusion Layer pH with Functionalized Gold Ultramicroelectrodes. Anal. Chem. 2020, 92, 2237–2243.
- (64) Zimer, A. M.; Medina da Silva, M.; Machado, E. G.; Varela, H.; Mascaro, L. H.; Pereira, E. C. Development of a Versatile Rotating Ring-Disc Electrode for In Situ pH Measurements. Anal. Chim. Acta 2015, 897, 17–23.
- (65) Zhang, F.; Co, A. C. Direct Evidence of Local pH Change and the Role of Alkali Cation during CO₂ Electroreduction in Aqueous Media. Angew. Chem. Int. Ed. 2020, 59, 1674–1681.
- (66) Fuladpanjeh-Hojaghan, B.; Elsutohy, M. M.; Kabanov, V.; Heyne, B.;

- Trifkovic, M.; Roberts, E. P. L. In-Operando Mapping of pH Distribution in Electrochemical Processes. *Angew. Chem. Inte. Ed.* **2019**, *58*, 16815–16819.
- (67) Monteiro, M. C.; Koper, M. T. Measuring Local pH in Electrochemistry. *Curr. Opin. Electrochem.* **2021**, *25*, 100649.
- (68) Wuttig, A.; Yaguchi, M.; Moto-bayashi, K.; Osawa, M.; Surendranath, Y. Inhibited Proton Transfer Enhances Au-Catalyzed CO₂-to-Fuels Selectivity. *Proc. Natl. Acad. Sci. U. S. A.* 2016, 113, E4585–E4593.
- (69) Singh, M. R.; Kwon, Y.; Lum, Y.; Ager, J. W.; Bell, A. T. Hydrolysis of Electrolyte Cations Enhances the Electrochemical Reduction of CO₂ over Ag and Cu. J. Am. Chem. Soc. 2016, 138, 13006– 13012.
- (70) Ayemoba, O.; Cuesta, A. Spectroscopic Evidence of Size-Dependent Buffering of Interfacial pH by Cation Hydrolysis during CO₂ Electroreduction. ACS Appl. Mater. Interfaces 2017, 9, 27377–27382.
- (71) Bondue, C. J.; Graf, M.; Goyal, A.; Koper, M. T. M. Suppression of Hydrogen Evolution in Acidic Electrolytes by Electrochemical CO₂ Reduction. J. Am. Chem. Soc. 2021, 143, 279–285.
- (72) Kim, C.; Weng, L.-C.; Bell, A. T. Impact of Pulsed Electrochemical Reduction of CO₂ on the Formation of C₂₊ Products over Cu. *ACS Catal.* **2020**, *10*, 12403–12413.
- (73) Han, Z.; Kortlever, R.; Chen, H.-Y.; Peters, J. C.; Agapie, T. CO₂ Reduction Selective for C_{≥2} Products on Polycrystalline Copper with N-Substituted Pyridinium Additives. ACS Cent. Sci. 2017, 3, 853–859.
- (74) Thevenon, A.; Rosas-Hernández, A.; Fontani Herreros, A. M.; Agapie, T.; Peters, J. C. Dramatic HER Suppression on Ag Electrodes via Molecular Films for

- Highly Selective CO2 to CO Reduction. *ACS Catal.* **2021**, *11*, 4530–4537.
- (75) Hall, A. S.; Yoon, Y.; Wuttig, A.; Surendranath, Y. Mesostructure-Induced Selectivity in CO₂ Reduction Catalysis. *J. Am. Chem. Soc.* 2015, 137, 14834–14837.
- (76) Gautam, R. P.; Lee, Y. T.; Herman, G. L.; Moreno, C. M.; Tse, E. C. M.; Barile, C. J. Controlling Proton and Electron Transfer Rates to Enhance the Activity of an Oxygen Reduction Electrocatalyst. Angew. Chem. Int. Ed. 2018, 57, 13480– 13483.
- (77) Barile, C. J.; Tse, E. C. M.; Li, Y.; Sobyra, T. B.; Zimmerman, S. C.; Hosseini, A.; Gewirth, A. A. Proton Switch for Modulating Oxygen Reduction by a Copper Electrocatalyst Embedded in a Hybrid Bilayer Membrane. *Nat. Mater.* **2014**, *13*, 619–623.
- (78) Ripatti, D. S.; Veltman, T. R.; Kanan, M. W. Carbon Monoxide Gas Diffusion Electrolysis that Produces Concentrated C₂ Products with High Single-Pass Conversion. *Joule* **2019**, *3*, 240–256.
- (79) Lu, X.; Zhu, C.; Wu, Z.; Xuan, J.; Francisco, J. S.; Wang, H. In Situ Observation of the pH Gradient near the Gas Diffusion Electrode of CO₂ Reduction in Alkaline Electrolyte. J. Am. Chem. Soc. **2020**, 142, 15438–15444.
- (80) Dinh, C.-T.; Burdyny, T.; Kibria, M. G.; Seifitokaldani, A.; Gabardo, C. M.; García de Arquer, F. P.; Kiani, A.; Edwards, J. P.; De Luna, P.; Bushuyev, O. S. et al. CO₂ Electroreduction to Ethylene via Hydroxide-Mediated Copper Catalysis at an Abrupt Interface. Science 2018, 360, 783-787.
- (81) Huang, J. E.; Li, F.; Ozden, A.; Sedighian Rasouli, A.; García de Arquer, F. P.; Liu, S.; Zhang, S.; Luo, M.; Wang, X.; Lum, Y. et al. CO₂ Electrolysis

to Multicarbon Products in Strong Acid. Science **2021**, 372, 1074.

Graphical TOC Entry

